Resonance Zones in Action Space

Jan Wiersig

Max-Planck-Institut für Physik komplexer Systeme, D-01187 Dresden

Reprint requests to Dr. J. W.; Fax: (+49) 351/871-1999; E-mail: jwiersig@mpipks-dresden.mpg.de

Z. Naturforsch. **57 a,** 537–556 (2001); received June 23, 2001

The classical and quantum mechanics of isolated, nonlinear resonances in integrable systems with $N \geq 2$ degrees of freedom is discussed in terms of geometry in the space of action variables. Energy surfaces and frequencies are calculated and graphically presented for invariant tori inside and outside the resonance zone. The quantum mechanical eigenvalues, computed in the semiclassical WKB approximation, show a regular pattern when transformed into the action space of the associated symmetry reduced system: eigenvalues inside the resonance zone are arranged on N-dimensional cubic lattices, whereas those outside are, in general, non-periodically distributed. However, N-dimensional triclinic (skewed) lattices exist locally. Both kinds of lattices are joined smoothly across the classical separatrix surface. The statements are illustrated with the help of two and three coupled rotors. The energy-level statistics of this system are found numerically to be in very good agreement with the Poisson distribution, despite of the complex lattice structure.
PACS: 03.65.Sq, 05.45.-a

Key words: Resonance Zones; Energy Surfaces; Action Space; Energy-level Statistics; Semiclassical Quantization.

1. Introduction

The surfaces of constant energy $H(\boldsymbol{I}) = E$ in the space of action variables $\boldsymbol{I} = (I_1, \ldots, I_N)$ contain the essential information about the dynamics of a compact integrable system, such as the fundamental frequencies $\boldsymbol{\omega} = \partial H/\partial \boldsymbol{I}$ and the foliation by invariant tori. The frequencies are given by the normals of the surfaces, whereas the foliation can be read off from the way an energy surface is divided into several patches, each representing a certain type of motion. "Simple systems" with trivial foliation like uncoupled harmonic oscillators have globally continuous and smooth energy surfaces. For many of the non-simple systems considered so far [1 - 9], the energy surfaces are nonsmooth at separatrices, but, nevertheless, continuous or can be made continuous by a reduction of the system's discrete symmetries. In [10, 11, 9] such systems are referred to as "one-component systems".

The subject of the present work is a class of one-component systems composed of integrable approximations of near-integrable systems of the form

$$H(\boldsymbol{J}, \boldsymbol{\varphi}) = H_0(\boldsymbol{J}) + \varepsilon H_1(\boldsymbol{J}, \boldsymbol{\varphi}) , \qquad (1)$$

where $\varepsilon > 0$ is the perturbation parameter, H_1 is a periodic function in the angles $\boldsymbol{\varphi}$, and H_0 describes the unperturbed system which is required to be simple in order to ensure that its action-angle variables $\boldsymbol{J}, \boldsymbol{\varphi}$ can be defined globally in phase space. The KAM theorem [12 - 14] states that a finite fraction of the unperturbed invariant tori survives smoothly deformed, namely those tori "sufficiently far" from resonance surfaces

$$\boldsymbol{m} \cdot \boldsymbol{\omega}_0(\boldsymbol{J}) = 0 , \qquad (2)$$

with relatively prime integer vectors $\boldsymbol{m}$ (an entire set $m_1, \ldots, m_N$ has no common divisor). The remaining fraction consists of chaotic trajectories, primary "islands" associated with the resonances of the unperturbed system (2) and higher-order islands. The smoothly deformed tori can be approximated by canonical perturbation theory. In the first order, the Hamiltonian (1) is averaged over the unperturbed tori, implicitly assuming that all angles $\boldsymbol{\varphi}$ are rapidly varying. Close to a primary island this assumption is not valid; the phase $\boldsymbol{m} \cdot \boldsymbol{\varphi}$ is almost stationary. Resonant perturbation theory [15] then suggests a better procedure: average over submanifolds of the unperturbed tori, $\boldsymbol{m} \cdot \boldsymbol{\varphi} = \text{const}$; expand the resulting integrable Hamiltonian

$$H(\boldsymbol{J}, \boldsymbol{\varphi}) = H_0(\boldsymbol{J}) + \varepsilon V(\boldsymbol{J}, \boldsymbol{m} \cdot \boldsymbol{\varphi}) \qquad (3)$$

0932–0784 / 01 / 0800–0537 $ 06.00

at the resonance surface in $\boldsymbol{J}$ and in a Fourier series in $\boldsymbol{\varphi}$, and retain only the most important contribution

$$V(\boldsymbol{J}, \boldsymbol{m} \cdot \boldsymbol{\varphi}) = f(\boldsymbol{J}) \cos(q\boldsymbol{m} \cdot \boldsymbol{\varphi}) , \tag{4}$$

where q is an integer. The regular dynamics in- and outside an isolated primary island described by the integrable Hamiltonian (3, 4) is well understood; see, e. g., [16]. Hamiltonians of this type have been frequently used as physical models, e.g., for energy transfer in triatomic molecules; see [17] and references therein. However, energy surfaces have only been presented for a special case with two degrees of freedom [3]. We here show the energy surfaces for a broader class of isolated-island systems with $N \geq 2$ degrees of freedom. Note that close to a resonance surface of higher codimension, i.e. where two or more resonance surfaces (2) meet each other, it can be necessary to include several terms of the form (4) into Hamilton's function. The dynamics will then be non-integrable and its analysis goes beyond the scope of this article.

Actions were the central ingredients for the old quantum mechanics before 1926. Bohr and Sommerfeld, among others, computed energy spectra by discretizing classical action integrals in integer multiples of $\hbar$, Planck's constant divided by 2π. The necessity of classical integrability was pointed out by Einstein, who formulated the quantization rules in terms of invariant tori and action variables [18]. Later, Brillouin derived from Schrödinger's equation that the quantization of actions is an approximation rigorously valid only in the (semi-)classical limit $\hbar \to 0$. Keller finally corrected this semiclassical approximation by Maslov indices in the presence of caustics [19]. According to the Einstein-Brillouin-Keller (EBK) rule, the quantization of an integrable system is a discretization of its action space by a N-dimensional cubic lattice with lattice constant $\hbar$. Unfortunately, this plain recipe only applies to simple systems because the presence of separatrices destroys the applicability of the EBK rule, and, more severely, there is in general no one-to-one correspondence between classical action variables and quantum eigenvalues [10]. However, the recipe can be extended to one-component systems by introducing the action space of the associated symmetry reduced system [10]. It has been found in [7, 20, 11] that the classical partition of this space into domains of different types of motion carries over to the discretization: away from the separatrix surfaces there exist N-dimensional cubic lattices, each related to the EBK rule for the corresponding type of motion; across the separatrix surfaces the lattices are smoothly connected. We here demonstrate that the Hamiltonian (3, 4) gives rise to novel, less symmetric eigenvalue lattices. We will see that this is due to an unusual and non-trivial kind of symmetry reduction which is more general than those used in [7, 20, 11].

The outline of the paper is as follows. In Sect. 2, we transform the Hamiltonian (3, 4) to a simpler form and expand it at the resonance surface in accordance to resonant perturbation theory. We then compute action variables and energy surfaces. The latter are graphically presented for a simple model, two and three coupled rotors. The section ends with a comparison to canonical perturbation theory. In Sect. 3, we firstly derive the semiclassical quantization condition, and then investigate the eigenvalue pattern in action space, illustrated with the help of the coupled-rotors model. The implications on the energy-level statistics are discussed at the end of this section. Finally, we briefly draw conclusions in Section 4.

2. Energy Surfaces in Action Space

2.1. Transformation to Standard Form

First of all, we transform the Hamiltonian (3) such that $\boldsymbol{m} \to (0, \ldots, 0, 1)$. If only one component of $\boldsymbol{m}$ is nonzero then this is achieved by redefining the indices. In the general case we first redefine the indices such that the first two components m_1, m_2 are nonzero and relatively prime. Second, we introduce new phase space variables $(\boldsymbol{P}, \boldsymbol{\vartheta})$ with one of the new angles $\vartheta_N = \boldsymbol{m} \cdot \boldsymbol{\varphi}$ being stationary at the resonance surface. For this purpose, we apply the generating function $F(\boldsymbol{\varphi}, \boldsymbol{P}) = \boldsymbol{P} \cdot Q\boldsymbol{\varphi}$ of Goldstein type 2 [21]. The relations $\boldsymbol{\vartheta} = \partial F / \partial \boldsymbol{P}$ and $\boldsymbol{J} = \partial F / \partial \boldsymbol{\varphi}$ give

$$\boldsymbol{P} = (Q^t)^{-1} \boldsymbol{J}, \ \boldsymbol{\vartheta} = Q\boldsymbol{\varphi} . \tag{5}$$

This transformation is not only canonical but also unimodular provided that the $N \times N$-matrix Q has integer-valued components and determinant ± 1 (For our purpose it is sufficient to consider matrices with determinant 1). This property ensures that $(\boldsymbol{P}, \boldsymbol{\vartheta})$ are action-angle variables of the unperturbed system. Remarkably, non-unimodular transformations are often used in the literature, even though the resulting variables are not action-angle variables in the sense

of Liouville-Arnol'd [22], i.e. fixing the actions and varying the angles independently from 0 to 2π does not yield a single complete cover of a torus. This has already been mentioned in [23] where a construction of the matrix Q has been given. We here make up a similar, but simpler matrix. For two-degrees-of-freedom systems we simply choose

$$Q_2 = \begin{pmatrix} d_2 & -d_1 \\ m_1 & m_2 \end{pmatrix}, \tag{6}$$

where d_1, d_2 are integers satisfying the diophantine equation

$$\det Q_2 = d_1 m_1 + d_2 m_2 = 1 \,. \tag{7}$$

It is known from number theory (see, e. g., [24]) that for given m_1, m_2, there exist a fundamental solution d_1, d_2, which can be calculated by Euclid's algorithm or chosen by hand. From this one gets a whole series of solutions $d_1(n) = d_1 - m_2\, n, d_2(n) = d_2 + m_1\, n$ with an integer n. With the matrix Q_2, the $(N-2)\times(N-2)$ unit matrix $\mathbf{1}_{N-2}$ and the $(N-2)\times 2$ matrix

$$W = \begin{pmatrix} 0 & \dots & 0 \\ m_3 & \dots & m_N \end{pmatrix} \tag{8}$$

we construct for more than two degrees of freedom the $N \times N$ matrix

$$Q = \begin{pmatrix} \mathbf{0} & \mathbf{1}_{N-2} \\ Q_2 & W \end{pmatrix}. \tag{9}$$

Using this matrix in transformation (5), Hamilton's function (3) takes the new form

$$\tilde{H}(\boldsymbol{P}, \vartheta_N) = \tilde{H}_0(\boldsymbol{P}) + \varepsilon\, \tilde{V}(\boldsymbol{P}, \vartheta_N) \,. \tag{10}$$

The tilde ˜ will be dropped henceforth. The angles $\vartheta_1, \dots, \vartheta_{N-1}$ do not appear in the new Hamiltonian. Hence, their conjugate momenta $P_1, \dots, P_{N-1}$ are constants of motion. As functions of the old momenta $\boldsymbol{J}$ only, they are in involution. The Hamiltonians (3) and (10) are therefore completely integrable. Action variables are introduced by means of

$$I_j = \frac{1}{2\pi} \oint_{\gamma_j} \boldsymbol{P}\, \mathrm{d}\boldsymbol{\vartheta} \,, \quad j = 1, \dots N \,. \tag{11}$$

With the transformation (5) being unimodular, a set of fundamental paths γ_j on a given invariant torus is determined by $\vartheta_i = \text{const}$, $i \neq j$. $N-1$ action integrals simply are $I_j = P_j$ if $j < N$, and it remains only one non-trivial integral,

$$I_N = \frac{1}{2\pi} \oint P_N\, \mathrm{d}\vartheta_N \,, \tag{12}$$

where P_N is regarded as a function of ϑ_N and the constants $E, P_1, \dots, P_{N-1}$.

2.2. *Expansion at the Resonance Surface*

The resonance surface in $\boldsymbol{P}$-space is given by $P_N = A(P_1, \dots, P_{N-1})$, where A is implicitly defined through $\dot{\vartheta}_N = \partial H_0 / \partial P_N = 0$. We expand the Hamiltonian (10) on this surface in the direction perpendicular to it. For this purpose, $|P_N - A|$ is assumed to be of order $\sqrt{\varepsilon}$, as usual in the analysis of resonances; see, e. g., [15, 16]. It is therefore sufficient to consider V as independent of P_N when expanding H in powers of $|P_N - A|$ to quadratic terms

$$\begin{aligned} H(\boldsymbol{P}, \vartheta_N) \;=\; & H_0(P_1, \dots, P_{N-1}, A) \\ & + \frac{1}{2} H_0''(P_1, \dots, P_{N-1}, A)(P_N - A)^2 \\ & + \varepsilon\, V(P_1, \dots, P_{N-1}, A, \vartheta_N) \,, \end{aligned} \tag{13}$$

where the prime $'$ denotes a derivative with respect to P_N. The local approximation (13) is useful provided $H_0'' \neq 0$ is fulfilled, which calls for a nonlinear dependence of H on P_N; this is why it is called "nonlinear resonance". It is illuminating to have a closer look at H_0'' in terms of the old coordinates

$$H_0'' = \boldsymbol{m} \cdot \frac{\partial \boldsymbol{\omega}_0}{\partial \boldsymbol{J}} \boldsymbol{m} \,, \tag{14}$$

where the Jacobian $\partial \boldsymbol{\omega}_0 / \partial \boldsymbol{J}$ is evaluated on the resonance surface. Note that, since (2) holds at resonance, $\boldsymbol{m}$ is a tangent to the unperturbed energy surface. Hence, H_0'' is the rate of frequency change on the energy surface perpendicular to the resonance surface or, equally, a measure of the curvature of the energy surface in the direction of $\boldsymbol{m}$. From this it is obvious that systems with planar unperturbed energy surfaces, like coupled harmonic oscillators, have to be treated separately.

Let us consider (13) as a one-degree-of-freedom Hamiltonian

$$H(P_N, \vartheta_N) = \frac{1}{2M}(P_N - A)^2 + E_0 + \varepsilon\, V(\vartheta_N). \tag{15}$$

The "mass" $M = 1/H_0''$ can be positive or negative. The zero level $E_0 = H_0$ does not affect the dynamics. It is worth mentioning that due to the "one-dimensional vector potential" A, the Hamiltonian (15) is not invariant under time reversal, which is $P_N \to -P_N$ when the other momenta are regarded as fixed parameters. We perform a further simplification, usually called "resonance-centre approximation", which ignores the dependence of the potential (4) upon the constants $P_1, \ldots, P_{N-1}$, i. e. $\tilde{f}(P_1, \ldots, P_{N-1}, A) \to f$. Absorbing $|f|$ in the perturbation parameter $\varepsilon > 0$ and using the freedom of shifting the angle $\vartheta_N \to \vartheta_N + \text{const}$, we take

$$V(\vartheta_N) = \text{sign}(M) \cos(q\vartheta_N) \,. \tag{16}$$

With $E_N = (E - E_0)\,\text{sign}(M)$ as the energy of the Nth degree of freedom, we get from energy conservation $H(P_N, \vartheta_N) = E$

$$P_N = \pm\sqrt{2|M|[E_N - \varepsilon\cos(q\vartheta_N)]} + A. \tag{17}$$

This is the textbook planar pendulum if $q = \varepsilon = 1$ and $A = 0$; see, e. g., [16] and for a quantum mechanical treatment see [25]. Inspection of Fig. 1a reveals that for general parameters the phase portrait differs from that of a pendulum in that there is a chain of q identical islands centred at $P_N = A$ instead of just a single island centred at $P_N = 0$. Let us specify briefly the invariant curves. At a fixed energy $E_N > \varepsilon$, there exist two invariant circles representing rotational-like motion (not necessarily related to physical rotations) with opposite sense of rotation $\Lambda = \text{sign}(\dot{\vartheta}_N) = \pm 1$, where $\dot{\vartheta}_N = P_N - A$. These circles are smooth deformations of the unperturbed ones. All other invariant objects, usually subsumed under the term "isolated resonance zone", are created by the perturbation: a separatrix and q unstable (hyperbolic) equilibrium points at the critical energy $E_N = \varepsilon$; q invariant "island circles" representing oscillatory motion in one of the potential wells labelled by $\Sigma = 1, \ldots, q$ at fixed $E_N \in (-\varepsilon, \varepsilon)$; q stable (elliptic) equilibrium points at the lowest energy $E_N = -\varepsilon$. It is to emphasize that the phase-space embedding of the island tori is topologically different from that of the smoothly deformed tori.

The system exhibits $2q$ discrete symmetries. It is invariant under reflections with respect to $\vartheta_N = (j-1)\pi/q$, $\Sigma = 1, \ldots, 2q$. These symmetries can be removed by implementing elastic reflections $\dot{\vartheta}_N \to -\dot{\vartheta}_N$ about $\vartheta_N = 0$ and $\vartheta_N = \pi/q$ as depicted in Figure 1b. This symmetry reduction restricts the oscillations to one half of the first potential well, whereas it converts the rotations to oscillations within the interval $[0, \pi/q]$.

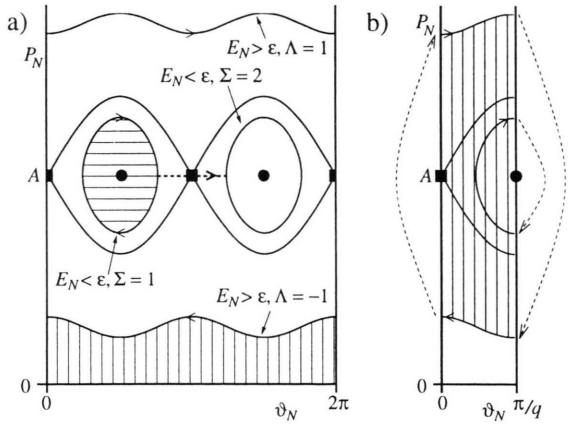

Fig. 1. a) Sketch of an isolated resonance zone with $q = 2$ in the (P_N, ϑ_N)-plane; see (17). The lines $\vartheta_N = 0$ and $\vartheta_N = 2\pi$ are identified. Shaded regions represent action integrals. Filled circles and squares mark stable and unstable equilibrium points, respectively. The thick dashed line is the integration path C_Θ of the tunnel integral specified in Section 3. b) Symmetry reduced resonance. Dashed lines symbolize elastic reflections.

2.3. *Actions and Energy Surfaces*

We now turn to the calculation of action variables. At fixed $E_N > \varepsilon$ and fixed Λ, the action integral (12) is the area in the (P_N, ϑ_N)-plane between the invariant circle and the line $P_N = 0$ as illustrated in Fig. 1a. We choose the closed integration path to be parametrized by ϑ_N increasing from 0 to 2π. The action I_N takes on positive as well as negative values depending on the sense of rotation $\Lambda = \pm 1$ and, remarkably, on A. At fixed $E_N < \varepsilon$, I_N is the area enclosed by the invariant circle. The chosen integration path lies inside a given potential well going from the left turning point ($\dot{\vartheta}_N = 0$) to the right one (along the $\dot{\vartheta}_N > 0$-branch) and back (along the $\dot{\vartheta}_N < 0$-branch). I_N is positive and the same for all wells. Please, pay attention to the fact that I_N changes discontinuously upon traversing the separatrix. As a consequence, there is no unique limiting action we could assign to the separatrix and the embedded unstable equilibrium points. Instead, there are three different actions arising from three

different energy limits, namely $E_N \to \varepsilon$ from below and $E_N \to \varepsilon$ with $\Lambda = \pm 1$ from above. This is in strong contrast to the continuous behaviour of the action $\tilde{I}_N$ of the symmetry reduced system; see Fig. 1b. At fixed $E_N < \varepsilon$, the integration path goes from the left turning point to the "solid wall" at $\vartheta_N = \pi/q$ and back after being reflected. With increasing energy, the left turning point wanders towards $\vartheta_N = 0$. Upon crossing the separatrix the smooth turning point is replaced by a reflection at $\vartheta_N = 0$. This does not spoil the continuity of $\tilde{I}_N$ (but its smoothness) since at $E_N > \varepsilon$ the action integral is the area between the two branches of the invariant circle ($P_N > A$ and $P_N < A$) as illustrated in Figure 1b. Note that $\tilde{I}_N$ does not depend on A as opposed to I_N. This is related to the remarkable fact that the symmetry reduction here does not only reduce phase space area by a factor, it also shifts its value by a constant. We call this a "non-trivial symmetry reduction".

The calculation of the action integrals is straightforward, and gives

$$\tilde{I}_N(E_N) = \begin{cases} \frac{2\sqrt{2}}{q\pi}\sqrt{|M|}\sqrt{E_N+\varepsilon}\,\mathcal{E}(1/k), \\ \qquad \text{if } E_N > \varepsilon, \\ \sqrt{\varepsilon}\frac{4}{q\pi}\sqrt{|M|}\left[\mathcal{E}(k) - (1-k^2)\mathcal{K}(k)\right], \\ \qquad \text{otherwise} \end{cases} \tag{18}$$

and

$$I_N(E_N) = \begin{cases} \Lambda q \tilde{I}_N + A, & \text{if } E_N > \varepsilon, \\ 2\tilde{I}_N, & \text{otherwise}, \end{cases} \tag{19}$$

where $\mathcal{K}(k)$ and $\mathcal{E}(k)$ are the complete elliptic integrals of first and second kind in the notation of [26, 27], with modulus $k^2 = (E_N/\varepsilon + 1)/2$. Let us now come back to the N-degrees-of-freedom system by noting that $\tilde{I}_j = I_j = P_j$ if $j < N$ (we do not care about further possible discrete symmetries). The system has the one-component property stemming from the continuity of $\tilde{I}_N$. This is mirrored by the geometrical fact that the two different regions of $\tilde{\boldsymbol{I}}$-space, the interior of the resonance zone with $E_N(\tilde{\boldsymbol{I}}) < \varepsilon$ and the exterior with $E_N(\tilde{\boldsymbol{I}}) > \varepsilon$, are continuously connected at the "separatrix surface" $E_N(\tilde{\boldsymbol{I}}) = \varepsilon$. The situation is more involved in $\boldsymbol{I}$-space. The interior of the resonance zone consists of q identical parts labelled by $\Sigma = 1, \ldots, q$. The exterior is made of two parts labelled by $\Lambda = \pm 1$ which are separated by a gap with size proportional to the square-root of the perturbation parameter,

$$\Delta I = 2q\tilde{I}_N(E_N = \varepsilon) = \sqrt{\varepsilon|M|}\frac{8}{\pi}\,. \tag{20}$$

A special situation occurs in the limit of vanishing perturbation strength. The resonance zone disappears, whereas its exterior coincides with the unperturbed action space after applying the inverse of transformation (5). It is therefore reasonable to subject this region to the inverse transformation also for finite perturbation, while keeping the other region as it is. This changes the set of fundamental paths only in the former region, which is allowed because the other region is separated by a separatrix which prevents a smooth continuation of fundamental paths anyway. We thus introduce new action variables as

$$\boldsymbol{L} = \begin{cases} \boldsymbol{I} & \text{inside the resonance zone} \\ Q^t\boldsymbol{I} & \text{outside.} \end{cases} \tag{21}$$

In $\boldsymbol{L}$-space, the gap between the two parts outside the resonance zone is

$$\Delta L = |\boldsymbol{m}|\Delta I = \sqrt{\varepsilon|M|}|\boldsymbol{m}|\frac{8}{\pi}\,. \tag{22}$$

Comparison with (14) brings to light that ΔL does not depend on the length of $\boldsymbol{m}$. Roughly speaking, ΔL is small (large) if the curvature of the energy surface in $\boldsymbol{m}$-direction is large (small).

The frequencies $\boldsymbol{\omega} = \partial H/\partial \boldsymbol{I}$ are calculated analogously as the actions giving

$$\omega_N = \text{sign}(M)\left(\frac{\partial I_N}{\partial E_N}\right)^{-1} \tag{23}$$

and

$$\omega_j = \begin{cases} \dfrac{\partial E_0}{\partial I_j} - (I_N - A)\dfrac{\omega_N}{2M}\dfrac{\partial M}{\partial I_j} - \omega_N\dfrac{\partial A}{\partial I_j}, \\ \qquad \text{if } E_N > \varepsilon, \\ \dfrac{\partial E_0}{\partial I_j} - I_N\dfrac{\omega_N}{2M}\dfrac{\partial M}{\partial I_j}, \\ \qquad \text{otherwise}, \end{cases} \tag{24}$$

with $j < N$.

2.4. *Example: Coupled Rotors*

Let us illustrate the previous considerations with an example of N coupled identical rotors described

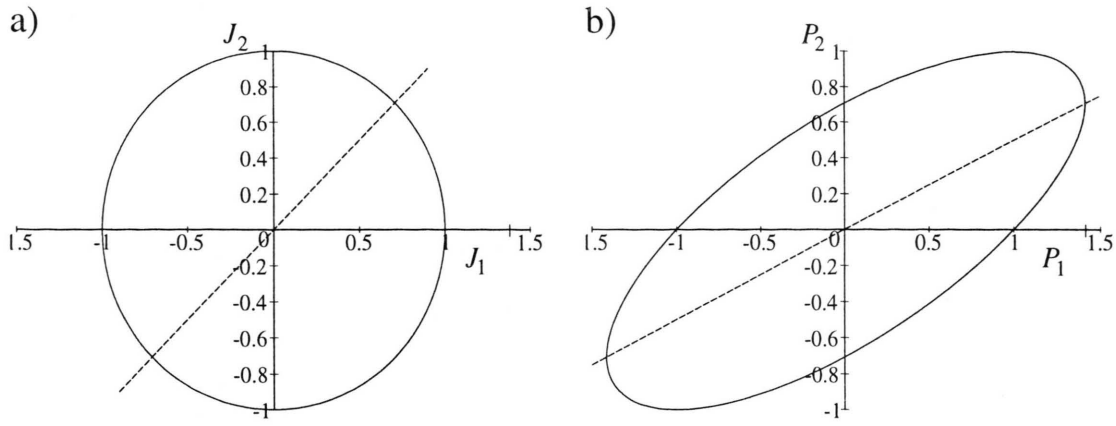

Fig. 2. (a) Energy surface $E = 1/2$ and $(-1, 1)$-resonance surface of two free rotors in $\boldsymbol{J}$-space; (b) transformed energy and $(0, 1)$-resonance surface in $\boldsymbol{P}$-space.

by the Hamiltonian

$$H(\boldsymbol{J}, \varphi) = \frac{1}{2}\boldsymbol{J}^2 + \varepsilon \cos(q\boldsymbol{m} \cdot \varphi) . \tag{25}$$

There is no need to expand this function; the unperturbed Hamiltonian $H_0 = \boldsymbol{J}^2/2 = \boldsymbol{J} \cdot \boldsymbol{J}/2$ is already a polynomial of second degree in $\boldsymbol{J}$ and the perturbation is independent of $\boldsymbol{J}$. The space of the unperturbed action $\boldsymbol{J}$ is foliated by $(N-1)$-dimensional concentric energy spheres $H_0(\boldsymbol{J}) = E$. The resonance surfaces $\boldsymbol{m} \cdot \boldsymbol{\omega}_0 = \boldsymbol{m} \cdot \boldsymbol{J} = 0$ form a dense set of $(N-1)$-dimensional planes passing through the origin. Figure 2a shows such surfaces for two degrees of freedom. The energy surface provides a comprehensive picture of the dynamics (free motion of two particles with coordinates φ_1 and φ_2 on a circle) at a fixed energy, in contrast to phase portraits as in Fig. 1 which contain only information about a single degree of freedom. The one-piece energy surface is present in all four quadrants of action space. From this we can infer the existence of only a single type of motion with two rotational degrees of freedom. Each point on the energy surface corresponds to an invariant 2-torus (a two-dimensional torus) in phase space with the outward normal being the torus' fundamental frequencies. The most important information contained in the two frequency components is their ratio, the winding number. A rational winding number indicates that the periods of the rotors are rationally related. For example, a $(-1, 1)$-resonance implies identical periods, so the particles move around the circle synchronously. In phase space, this motion is a periodic orbit. The time-independent phase difference $\varphi_2 - \varphi_1$ parametrizes a one-parameter family of such periodic orbits, forming a resonant 2-torus. These resonant tori are located on resonance surfaces in action space. For two degrees of freedom, the resonance surfaces are one-dimensional (see Fig. 2a) but we nevertheless refer to them as "surfaces". Resonances are of great importance due to their sensitivity to perturbations. Under general perturbations, chaotic motion spreads out from resonances (and separatrices).

For some special $\boldsymbol{m}$ with $q = 1$, the coupled-rotor model has a simple physical interpretation. First, if all numbers $m_1, \ldots, m_N$ are zero except m_j, the perturbation can be regarded as an harmonic potential of a spring connecting particle j with a fixed point on the circle. Note that the spring has a "negative spring constant" for positive ε. Second, $m_i = 1$, $m_j = -1$ and all other components vanishing models a spring between particle i and particle j. We discuss this case for two degrees of freedom in more detail. In order to have a unimodular transformation (5) with $\boldsymbol{m} = (-1, 1)$, we choose $(d_1, d_2) = (0, 1)$ leading to $M = 1/2$, $A = P_1/2$, and $E_0 = P_1^2/4$. The new angle ϑ_1 is equal to the old angle φ_1 and $\vartheta_2 = \varphi_2 - \varphi_1$ describes the relative motion of the two rotors. It is worth mentioning that the most intuitive transformation, relative coordinate ϑ_2 and "centre of mass" coordinate $\vartheta_1 = \varphi_1 + \varphi_2$ or $\vartheta_1 = (\varphi_1 + \varphi_2)/2$, is not unimodular. Yet, it is essential that the transformation (5) is unimodular, otherwise the normals of the

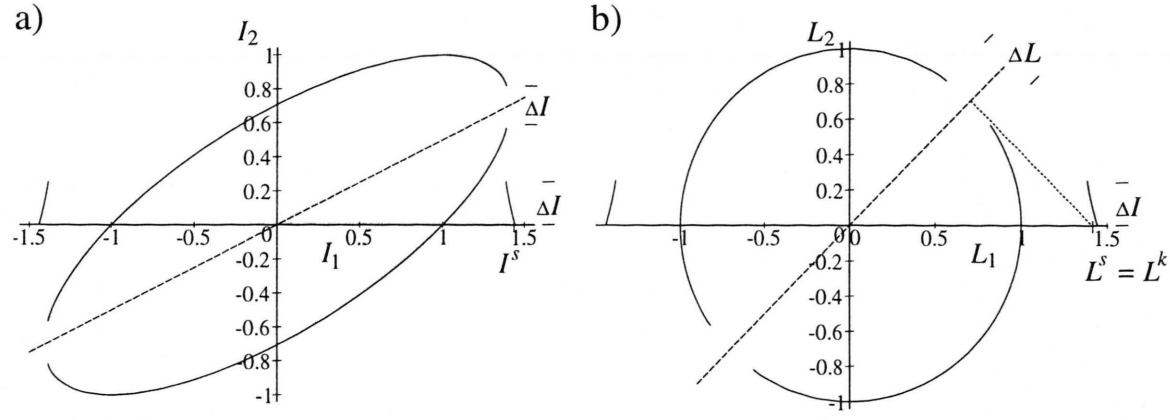

Fig. 3. Energy surface $E = 1/2$ of two coupled rotors with $\boldsymbol{m} = (-1, 1)$, $q = 1$, and $\varepsilon = 0.02$ in $\boldsymbol{I}$- (a) and $\boldsymbol{L}$-space (b). The dashed lines indicate the (0, 1)- (a) and the $(-1, 1)$-resonance (b) of the unperturbed system. The dotted line serves for the construction of the quantity L^k.

transformed energy surface plotted in Fig. 2b would not give the fundamental frequencies of the motion on tori. Note that the $(-1, 1)$-resonance ($\dot{\varphi}_2 - \dot{\varphi}_1 = 0$) is transformed into a (0, 1)-resonance ($\dot{\vartheta}_2 = 0$).

Both energy surfaces in Fig. 2 are borderless which is quite an untypical feature in the class of systems studied so far. Ordinary energy surfaces of two-degrees-of-freedom systems consist of different patches bounded by critical points. The critical points are related to isolated periodic orbits, indicating bifurcations of invariant tori. A critical point is called elliptic or hyperbolic depending on whether the periodic orbit is stable or unstable [8]. At an unstable orbit which is always accompanied by a separatrix the energy surface has a singular curvature at the critical point. It is natural that one action is zero at a stable orbit [3]. This can be achieved by a proper choice of fundamental paths on the invariant tori.

The perturbed energy surface in $\boldsymbol{I}$-space is calculated according to (18, 19) by fixing the energy E and varying the momenta $P_1, \ldots, P_{N-1}$. The result shown in Fig. 3a is an energy surface which consists of four patches and is more generic than the unperturbed one. The isolated resonance zone appears with two small symmetric patches with $|I_1| \geq I^s = 2\sqrt{E - \varepsilon}$ which are related by time reversal. A point on these patches belongs to an island torus where the old angle ϑ_2 describes oscillations, so only positive values of I_2 are meaningful. The two hyperbolic points with $(|I_1|, I_2) = (I^s, \Delta I = \sqrt{2\varepsilon}\, 4/\pi)$ mark unstable periodic orbits, clockwise and anti-clockwise rotating with $\vartheta_2 = \dot{\vartheta}_2 = 0$, and separatrix motion, which is asymptotic to the embedded unstable periodic orbit. The two elliptic points with maximum $|I_1|$ and $I_2 = 0$ characterize stable periodic orbits, clockwise and anti-clockwise rotating with $\vartheta_2 = \pi$, $\dot{\vartheta}_2 = 0$. Outside the resonance zone there exist two patches provided that $E > \varepsilon$. If $E \gg \varepsilon$ as in Fig. 3a, both patches together look like the unperturbed energy surface in $\boldsymbol{P}$-space shown in Fig. 2b, apart from the gap of size ΔI where the unperturbed surface has the (0, 1)-resonance. Points on these patches correspond to rotational motion similar to the unperturbed motion with both old angles ϑ_1 and ϑ_2 covering the entire interval $[0, 2\pi)$. The perturbation just lifts the constance of the velocities $\dot{\vartheta}_1$ and $\dot{\vartheta}_2$. The patches are bounded by two pairs of hyperbolic points with $I_1 = \pm I^s$. Each pair is related to one of the unstable periodic orbits and separatrices discussed above. Elliptic points do not exist.

Figure 3b displays the energy surface after transformation (21) is applied. Its rough features are captured by the following slight modification of the unperturbed energy surface in Fig. 2a: cut in holes of size $\Delta L = \sqrt{\varepsilon}\, 8/\pi$ at the $(-1, 1)$-resonance surface; draw a line from the intersection point of the resonance and energy surfaces tangential to the energy surface as pictured in Fig. 3b; its intersection point with the L_1-axis, L^k, is related to L^s via

$$L^s = |m_2 L^k| \,; \tag{26}$$

add two, almost vertical pieces of height ΔI at $|L_1| =$

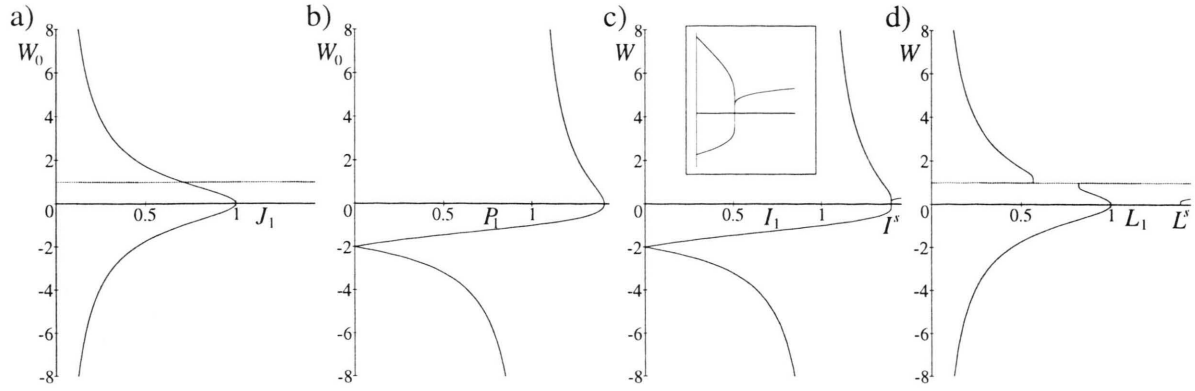

Fig. 4. Winding number of two coupled rotors with $E = 1/2$, $\boldsymbol{m} = (-1, 1)$, and $q = 1$. The symmetric regime of negative actions is omitted. a) Winding number $W_0(E, J_1)$ of the unperturbed system. The dotted line indicate the resonance $W_0(E, J_1) = 1$. b) $W_0(E, P_1)$. c) $W(E, I_1)$ with $\varepsilon = 0.02$. Inset: neighbourhood of the separatrix $I_1 = I^s$. d) $W(E, L_1)$.

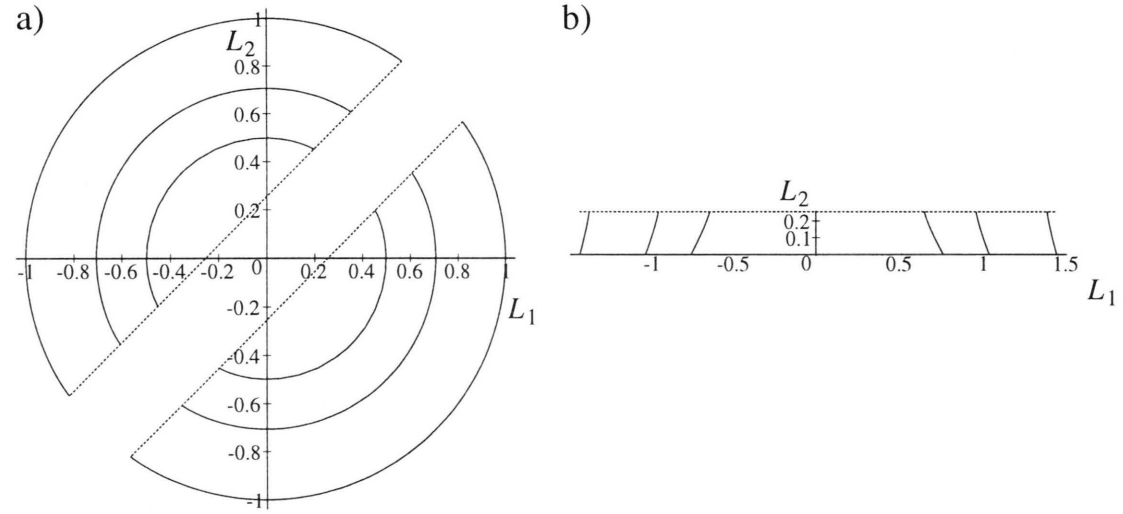

Fig. 5. Energy surfaces $E = 1/2, 1/4, 1/8$ of two coupled rotors with $\boldsymbol{m} = (-1, 1)$, $q = 1$, and $\varepsilon = 0.02$ outside (a) and inside (b) the resonance zone. The dotted lines mark the separatrix surface.

$L^s = I^s$. In our example with $m_2 = 1$ the quantities L^s and L^k are equal. In general, $L^s \geq L^k$.

The fine structure of the perturbed energy surface is illustrated in Fig. 4 with the help of the winding number. The unperturbed winding number $W_0 = \dot{\varphi}_2/\dot{\varphi}_1$ is simply $\pm\sqrt{2E - J_1^2}/J_1$. The $(-1, 1)$-resonance is characterized by $W_0(E, J_1) = 1$. The same resonance in $\boldsymbol{P}$-space is given by $W_0(E, P_1) = \dot{\vartheta}_2/\dot{\vartheta}_1 = 0$. Comparison of Figs. 4b and 4c shows that the winding number $W(E, I_1)$ at finite ε does not differ much from $W_0(E, P_1)$, apart from a new piece inside the resonance zone, which takes on small values of order $\sqrt{\varepsilon}$. The behaviour at the separatrix $I_1 = I^s$ can be seen more clearly in the magnification. Exactly at the separatrix, $W(E, I_1)$ logarithmically approaches zero, or, taking a more common point of view, $1/W(E, I_1)$ diverges logarithmically. This means, on the one hand, that the associated unstable motion can be regarded as resonant. On the other hand, it means that even though there is a gap in the energy surface, there is no such gap in the spectrum of the winding number. It can be inferred from Fig. 4d that this is also true for the transformed winding number $W(E, L_1)$. It approaches the

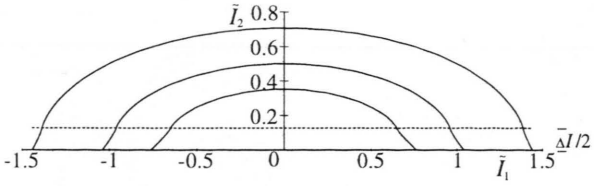

Fig. 6. Energy surfaces $E = 1/2, 1/4, 1/8$ of two symmetry reduced coupled rotors with $\boldsymbol{m} = (-1, 1)$, $q = 1$, and $\varepsilon = 0.02$. The dotted line marks the separatrix surface.

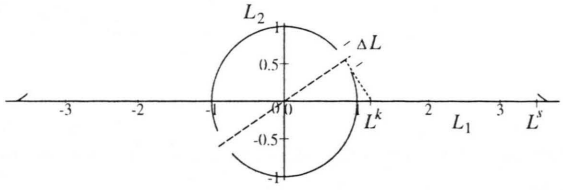

Fig. 7. Energy surface $E = 1/2$ of two coupled rotors with $\boldsymbol{m} = (-2, 3)$, $q = 2$, and $\varepsilon = 0.02$. The dashed line marks the $(-2, 3)$-resonance of the unperturbed system. The dotted line serves for the construction of the quantity L^k.

value 1 (in general $-m_2/m_1$) at the separatrix. The derivative of the winding number is large in the vicinity of the separatrix. As a consequence, there is an accumulation of low-order resonances (W is a fraction of two integers with small denominator) near the separatrix.

Figure 5 shows how the $\boldsymbol{L}$-space is foliated by energy surfaces. The evident discontinuity differs strongly from the continuity of $\tilde{\boldsymbol{I}}$-space, cf. Figs. 5 and 6. Let us try to get more familiar with the symmetry reduction on the basis of the model of two rotors coupled by a spring, $\boldsymbol{m} = (-1, 1)$ and $q = 1$. The symmetry-reducing reflections about $\vartheta_2 = 0$ and $\vartheta_2 = \pi$ are related to two symmetry transformations, $\vartheta_2 \to -\vartheta_2$ and $\vartheta_2 - \pi \to \pi - \vartheta_2$. The first one reads in the old angles: $\varphi_2 - \varphi_1 \to \varphi_1 - \varphi_2$. This is an interchange of particle 1 and 2, so the reflection at $\vartheta_2 = 0$ can be viewed as an elastic reflection between both particles. The interpretation of the second symmetry transformation, $\varphi_2 - (\varphi_1 + \pi) \to (\varphi_1 + \pi) - \varphi_2$, is more involved: shift particle 1 by π on the circle; interchange both particles and finally shift particle 1 by $-\pi$. The reflection at $\vartheta_2 = \pi$ can be seen as an elastic reflection of particle 2 with particle 1 virtually displaced by π.

Let us take a brief look at an example with $m_2, q > 1$, namely $\boldsymbol{m} = (-2, 3)$ and $q = 2$ with $(d_1, d_2) = (1, 1)$. We observe from Fig. 7 that the

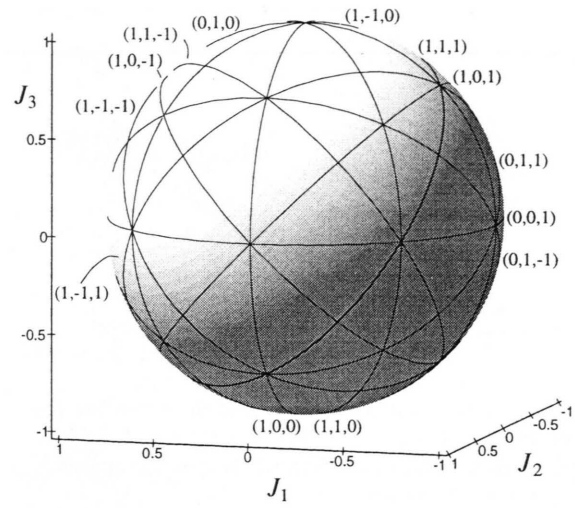

Fig. 8. Energy surface $E = 1/2$ of three free rotors in $\boldsymbol{J}$-space. Intersection lines with (m_1, m_2, m_3)-resonance surfaces, $|m_j| \leq 1$, are shown.

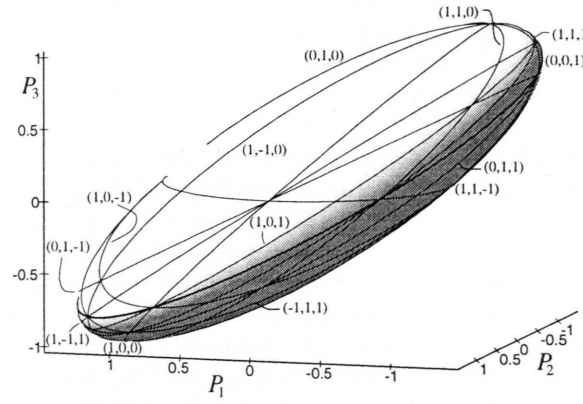

Fig. 9. Energy surface $E = 1/2$ of three free rotors in $\boldsymbol{P}$-space.

energy patches are well separated as predicted by (26). A point within the resonance zone represents two 2-tori, each a combination of a ϑ_1-rotation and a ϑ_2-oscillation in one of the two potential wells.

The description of the two-degrees-of-freedom dynamics extends to three (and more) degrees of freedom in a natural way. We demonstrate this with three coupled rotors, using $\boldsymbol{m} = (1, 1, 1)$, $q = 1$ and $(d_1, d_2) = (0, 1)$. Figure 8 shows that the unperturbed energy surface is made of a single piece being present in all octants of action space, so only one type of motion exists with three rotational degrees of freedom. Again, the surface is somewhat special in that it is

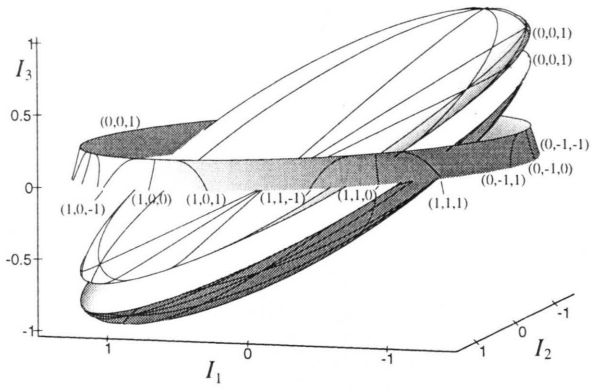

Fig. 10. Energy surface $E = 1/2$ of three coupled rotors with $\boldsymbol{m} = (1, 1, 1)$, $q = 1$, and $\varepsilon = 0.02$ in $\boldsymbol{I}$-space. The unmarked resonances can be read off from the unperturbed energy surface in Figure 9.

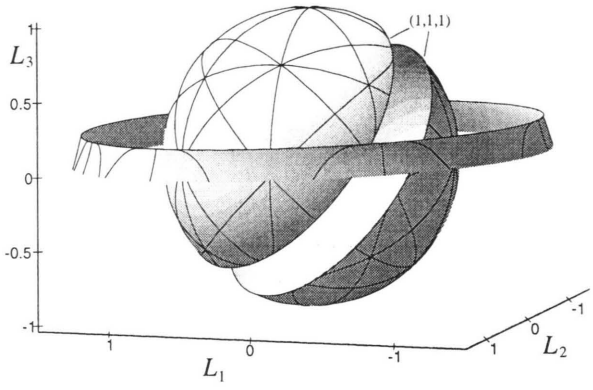

Fig. 11. Energy surface $E = 1/2$ of three coupled rotors with $\boldsymbol{m} = (1, 1, 1)$, $q = 1$, and $\varepsilon = 0.02$ in $\boldsymbol{L}$-space. The unmarked resonances can be read off from the unperturbed energy surfaces in Figs. 8 and 10.

borderless. Typical energy surfaces of three-degrees-of-freedom systems are composed of several patches bounded by critical edges. Interior points of a given patch represent 3-tori. Elliptic edges correspond to stable isolated 2-tori, whereas hyperbolic edges correspond to unstable isolated 2-tori and separatrices. Corner points represent isolated periodic orbits and separatrices. Although isolated low-dimensional tori do not exist in the free-rotor model, there are families of low-dimensional tori on resonance surfaces. Figure 8 reveals that these surfaces intersect a spherical energy surface in great circle meridians. All intersection lines together form a dense set, the so-called Arnold web. Along intersection lines we find resonant 3-tori, one-parameter families of 2-tori. A torus at an intersection point of two such lines (a resonance of higher codimension) is completely resonant, i. e. it is foliated by periodic orbits. The resonance surfaces are shown in Fig. 8 up to order one, i. e. $|m_j| \leq 1$. Note that the order so defined is not invariant under unimodular transformations. The resonances on the energy sphere in Fig. 8 and the transformed surface in Fig. 9 are therefore not always related via transformation (5).

Figures 10 and 11 illustrate how the perturbation modifies the energy surfaces in 3D action space. Let us concentrate on the $\boldsymbol{L}$-representation in the latter figure. The resonance zone cylindrically surrounds the other parts of the energy surface. Its elliptic edge in the plane $L_3 = 0$ presents isolated stable 2-tori. Such a torus is essentially a direct product of a circle and the stable periodic orbit discussed for two degrees of freedom. The other edge is hyperbolic and $(0, 0, 1)$-resonant. Its unstable 2-tori and separatrices are again direct products of a circle with the corresponding two-degrees-of-freedom object. The resonance zone has no corner points and, correspondingly, no isolated periodic orbits. The energy surface outside the resonance zone is torn open along the $(1, 1, 1)$-resonance surface of the unperturbed system; cf. Figs. 8 and 11. Apart from this gap, the shape of the surface is again similar to that of the unperturbed surface. The hardly visible deformation close to the gap is uncovered by the graphical representation of resonances. The two hyperbolic edges are special $(1, 1, 1)$-resonances which are tangentially approached by other resonances. This is analogous to the earlier-mentioned accumulation of resonances in the vicinity of separatrices in the case of two degrees of freedom.

2.5. *Comparison with Canonical Perturbation Theory*

Having calculated the energy surfaces of coupled rotors exactly, we now compare them to approximated surfaces. Canonical perturbation theory applies near-identity transformations parametrized by ε to the action-angle variables such that the new Hamiltonian is independent of the angles and therefore integrable; see, e. g., [16]. After eighth-order canonical perturbation theory the Hamiltonian (25) transforms to

$$H_{\mathrm{app}}(\boldsymbol{L}) = \frac{1}{2}\boldsymbol{L}^2 + \varepsilon^2\frac{1}{4}\xi^2 + \varepsilon^4\frac{5}{64}\xi^6 + \varepsilon^6\frac{9}{128}\xi^{10} + \varepsilon^8\frac{1469}{16384}\xi^{14} \tag{27}$$

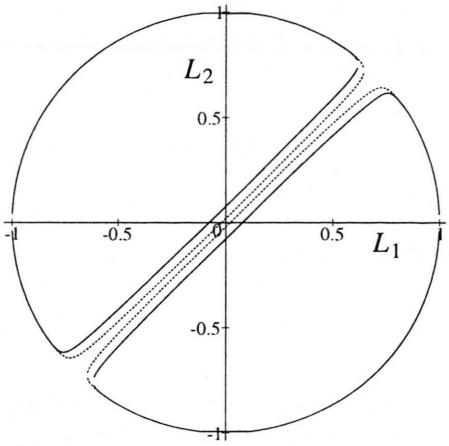

Fig. 12. Energy surface $E = 1/2$ of two coupled rotors with $\boldsymbol{m} = (-1, 1)$, $q = 1$, and $\varepsilon = 0.02$ in second-order (dotted) and fourth-order (solid) canonical perturbation theory; compare with the exact surface in Figs. 3b and the unperturbed surface in Figure 2a.

with the new actions $\boldsymbol{L}$ and the abbreviation $\xi = |\boldsymbol{m}|/(\boldsymbol{m} \cdot \boldsymbol{L})$. It turns out that $H_{\text{app}}(\boldsymbol{L})$ agrees with the Taylor series of $H(\boldsymbol{L})$ for $E_N > \varepsilon$ which is obtained from expanding (18, 19) in powers of ε, transforming according to (21), and solving (to eighth order) for the energy. Hence, canonical perturbation theory approximates the energy surfaces outside the resonance zone, cf. Figs. 3b and 12. But notice that $H_{\text{app}}(\boldsymbol{L})$ diverges on the resonance surface of the unperturbed system, $\boldsymbol{m} \cdot \boldsymbol{L} = 0$. This is responsible for the fact that the approximate energy surfaces do not have hyperbolic boundaries but instead additional segments close to the resonance surface without any physical interpretation!

The energy surfaces within the resonance zone cannot be approximated in this way. The reason is that the near-identity transformations cannot cope with the different topology of the phase-space embedding of island tori; see, e. g., [16]. We arrive at the same conclusion by observing that for $E_N < \varepsilon$ the action I_N in (18, 19) cannot be expanded in a Taylor series in powers of ε.

3. Discretization of Action Space

3.1. Semiclassical Quantization Condition

It is instructive to begin with the EBK rule of the unperturbed system,

$$\boldsymbol{J} = (\boldsymbol{k} + \boldsymbol{\beta}/4)\hbar \,, \tag{28}$$

with quantum numbers $\boldsymbol{k}$ and Maslov indices $\boldsymbol{\beta}$. The latter are classical indices characterizing the motion on a given invariant torus: $\beta_j = 0$ if the jth degree of freedom is of rotational type and $\beta_j = 2$ if the jth degree of freedom is of oscillatory type [19, 28]. For rotational motion, J_j and k_j assume positive as well as negative values (example: angular momentum in a system with rotational symmetry), whereas for oscillatory motion, both numbers are usually restricted to non-negative values (example: one-dimensional harmonic oscillator). A Hamilton operator $\hat{H}_0$ with semiclassical eigenfunctions

$$\psi_k(\boldsymbol{\varphi}, \varepsilon = 0) \propto \exp[i(\boldsymbol{k} + \boldsymbol{\beta}/4) \cdot \boldsymbol{\varphi}] \tag{29}$$

can be obtained from the unperturbed Hamilton's function H_0 with the usual operator replacement $J_j \to -i\hbar\partial/\partial\varphi_j$, $j = 1, \ldots, N$ and $i^2 = -1$. The semiclassical eigenvalues of $\hat{H}_0$ are $E = H_0(\boldsymbol{J})$ with $\boldsymbol{J}$ from (28). Note that the functions (29) are in general not 2π-periodic in the angles φ_j. This stems from the singularities in the transformation from the original Cartesian coordinates $\boldsymbol{x}$ and momenta $\boldsymbol{p}$ to action-angle variables. Transforming the functions (29) according to (5) results in

$$\psi_n(\boldsymbol{\vartheta}, \varepsilon = 0) \propto \exp[i(\boldsymbol{n} + \boldsymbol{\alpha}/4) \cdot \boldsymbol{\vartheta}] \tag{30}$$

with new quantum numbers $\boldsymbol{n} = (Q^{-1})^t \boldsymbol{k}$ and Maslov indices $\boldsymbol{\alpha} = (Q^{-1})^t \boldsymbol{\beta}$. We see here again that it is important to employ a unimodular transformation; it guarantees that n_j and α_j are integer-valued and that consecutive values of n_j differ by 1.

The EBK rule cannot be applied to the perturbed system (3, 4) because the actions and Maslov indices are not globally defined for the entire phase space; their definition is different for the interior and the exterior of the isolated resonance. We need a quantization condition which is uniformly valid for the entire phase space. Our derivation of this uniform quantization condition is similar to the derivation in [29] but differs in three respects: an arbitrary number of degrees of freedom is allowed; the potential (4) has to be independent of $P_1, \ldots, P_{N-1}$; action-angle variables are used at every stage. Let us start from the ansatz

$$\psi_n(\boldsymbol{\vartheta}) \propto \exp\left[i \sum_{j=1}^{N-1} (n_j + \alpha_j/4)\vartheta_j\right] \psi(\vartheta_N, n_N) \tag{31}$$

with the eigenfunction of the Nth degree of freedom

$$\psi(\vartheta_N, n_N) = \exp[i(\alpha_N/4)\vartheta_N]\ \Omega(\vartheta_N, n_N). \quad (32)$$

The function $\Omega(\vartheta_N, n_N)$ is to be 2π-periodic in ϑ_N in order to ensure $\Omega(\vartheta_N, n_N) \to \exp(in_N\vartheta_N)$ and $\psi_n(\boldsymbol{\vartheta}) \to \psi_n(\boldsymbol{\vartheta}, \varepsilon = 0)$ as $\varepsilon \to 0$. Clearly, $N-1$ degrees of freedom in these variables are quantized à la EBK,

$$I_j = P_j = (n_j + \alpha_j/4)\hbar,\ j = 1, \ldots, N-1\ . \quad (33)$$

In order to find a quantization condition for the remaining degree of freedom we insert the conditions (33) and $P_N \to -i\hbar\partial/\partial\vartheta_N$ in Hamilton's function (15), leading to a Hamilton operator with eigenvalue equation

$$\left[\frac{1}{2M}\left(-i\hbar\frac{\mathrm{d}}{\mathrm{d}\vartheta_N} - A\right)^2 + E_0 - E + \varepsilon V(\vartheta_N)\right] \quad (34)$$

$$\cdot\, \psi(\vartheta_N, n_N) = 0.$$

With the Bloch-wave ansatz

$$\psi(\vartheta_N, n_N) = \exp(iA\vartheta_N/\hbar)\, \Psi(\vartheta_N, n_N) \quad (35)$$

a Schrödinger equation without "vector potential" A is obtained:

$$\left[-\frac{\hbar^2}{2M}\frac{\mathrm{d}^2}{\mathrm{d}\vartheta_N^2} + E_0 - E + \varepsilon V(\vartheta_N)\right]\Psi(\vartheta_N, n_N) = 0. \quad (36)$$

The wave functions $\Psi(\vartheta_N, n_N)$ fulfill "twisted boundary conditions"

$$\Psi(\vartheta_N + 2\pi, n_N) = \exp(2\pi i\sigma)\, \Psi(\vartheta_N, n_N) \quad (37)$$

with the real quantity

$$\sigma = -A(I_1, \ldots, I_{N-1})/\hbar + \alpha_N/4 \quad (38)$$

and $\mathrm{d}\Psi/\mathrm{d}\vartheta_N$ continuous. With the potential (16) ($|f|$ is again absorbed in ε) we finally get

$$\left[-\frac{\hbar^2}{2|M|}\frac{\mathrm{d}^2}{\mathrm{d}\vartheta_N^2} - E_N + \varepsilon\cos(q\vartheta_N)\right]\Psi(\vartheta_N, n_N) = 0. \quad (39)$$

According to [30], the semiclassical solutions E_N of this eigenvalue problem with boundary conditions (37) are given by

$$\cos(\phi - \rho) = \frac{\cos[2\pi(l-\sigma)/q]}{\sqrt{1 + \exp(2\Theta/\hbar)}},\ l = 1, \ldots, q. \quad (40)$$

Let us specify the constituents of this formula. The first one is the phase integral

$$\phi(E_N) = \frac{1}{\hbar}\int_{C_\phi} P_N\, \mathrm{d}\vartheta_N. \quad (41)$$

At fixed $E_N < \varepsilon$, the integration path C_ϕ connects the turning points inside a potential well. At $E_N > \varepsilon$, the path goes from $\vartheta_N = 0$ to $\vartheta_N = 2\pi/q$. It is an easy exercise to show that the phase integral is related to the action integrals (18) by means of $\phi = 2\pi\tilde{I}_N/\hbar$. The path C_ϕ lies entirely in the classically allowed region of phase space, in contrast to the integration path of the tunnel integral

$$\Theta(E_N) = -i\int_{C_\Theta} P_N\, \mathrm{d}\vartheta_N\ , \quad (42)$$

which lies in classically forbidden regions. At fixed $E_N < \varepsilon$, the path C_Θ links turning points from neighbouring potential wells through the barrier as shown in Figure 1a. In this case the tunnel integral of the barrier is positive. At $E_N > \varepsilon$, the path connects complex turning points, which are complex conjugates of each other, yielding a negative tunnel integral. Again we show directly the outcome of the calculation:

$$\Theta = \begin{cases} \dfrac{8\sqrt{\varepsilon}}{q}\sqrt{|M|}k\ \left[\mathcal{E}(\sqrt{k^2-1}/k) - \mathcal{K}(\sqrt{k^2-1}/k)\right] \\ \qquad \text{for } E_N > \varepsilon, \\ \dfrac{8\sqrt{\varepsilon}}{q}\sqrt{|M|}\left[\mathcal{E}(\sqrt{1-k^2}) - k^2\mathcal{K}(\sqrt{1-k^2})\right] \\ \qquad \text{otherwise,} \end{cases} \quad (43)$$

where k is the same modulus as for the action variable (18, 19). ρ is the "quantum correction function"

$$\rho(E_N) = -\frac{\Theta}{2\pi}\log\left[1 + \left(\frac{e\pi\hbar}{4\beta\Theta}\right)^2\right] \quad (44)$$

with $e = \exp(1)$ and $\beta = 1.78107$. A detailed derivation of the formula (40) based on a WKB ansatz can be found in [31]. Note that even though the WKB method is only valid in the semiclassical limit $\hbar \to 0$,

or to put it another way, for highly excited states, it gives very often accurate results even for the ground state. We mention that an equivalent quantization condition (up to corrections of higher order in $\hbar$) could be introduced by investigating the asymptotics of the solutions of Schrödinger's equation close to the separatrix. This has been carried out for the elliptic billiard in [32] and used in [33] (see also [20]) to derive a trace formula in terms of periodic orbits which is valid in the presence of a separatrix.

For solving the quantization condition (40) it is convenient to use a combination of bisection and Newton's method. Firstly, the actions $\tilde{I}_1, \ldots, \tilde{I}_{N-1}$ are determined from the given numbers $n_1, \ldots, n_{N-1}$ by virtue of the rules (33). Secondly, the minimum energy $e_0 = E_0(\tilde{I}_1, \ldots, \tilde{I}_{N-1}) - \mathrm{sign}(M)\varepsilon$ with $\phi(e_0) = 0$ is computed. Thirdly, the running index j is initialized to 0. Fourthly, we look for an energy e_{j+1} such that the interval (e_j, e_{j+1}) includes exactly one eigenvalue. To do so, we note that the left hand side of condition (40) is essentially a cosine of ϕ (ρ can be ignored for the following arguments) and that the right hand side and ϕ are monotonic functions of the energy. Hence, a suitable energy e_{j+1} is given implicitly by the relation $\phi(e_{j+1}) = j\pi$ which is solved numerically with Newton's method taking e_j as starting value. Having determined the interval, the bisection method is employed to find the enclosed eigenvalue. Finally, j is increased by one and the last steps are repeated until the desired number of eigenvalues is found.

3.2. *Lattice Structure*

An analogy between action-space discretization and crystal lattices can be drawn by rewriting the EBK rule for the unperturbed system (28) as

$$\boldsymbol{J} = \boldsymbol{a}_0 + \sum_{i=1}^{N} k_i \boldsymbol{a}_i \tag{45}$$

with basis vector $\boldsymbol{a}_0 = \beta\hbar/4$ and primitive lattice vectors $a_{ij} = \delta_{ij}\hbar$, where δ_{ij} is the Kronecker symbol. Equation (45) defines a lattice in $\boldsymbol{J}$-space, the primitive elementary cell of which is an N-dimensional cube with side length $\hbar$. What kind of lattice does the quantization condition (40) imply? According to [20], we formulate the quantization condition in terms of the action variables of the symmetry reduced system $\tilde{\boldsymbol{I}}$. This is trivial for the phase integral $\phi = 2\pi\tilde{I}_N/\hbar$, but the relation $E_N = E_N(\tilde{I}_N)$ has to be computed numerically. Note that the relation is unique and continuous due to the one-component property; see also [10]. The tunnel integral and the quantum correction function become functions of $\tilde{I}_N$ via $E_N = E_N(\tilde{I}_N)$. We observe that the quantization condition (40) is a function of the actions $\tilde{\boldsymbol{I}}$ alone. It is essential to realize that we cannot replace the actions of the symmetry reduced system $\tilde{\boldsymbol{I}}$ by the actions of the full system $\boldsymbol{I}$ using (19) since the classical index Λ is not provided by quantum mechanics. Quantum mechanically, we cannot distinguish between a classical torus with $\Lambda = +1$ and its symmetric partner with $\Lambda = -1$. This is the reason for the importance of the action space of the associated symmetry reduced system.

The quantization condition (40) has two solutions with the same quantum number l in each $\tilde{I}_N$-interval of width $\hbar$. We therefore add two further quantum numbers, $\Pi = \pm 1$ and $\tilde{n}_N = 0, 1, 2, \ldots$. The former distinguishes both solutions and the latter labels the intervals. We then verify that the quantization condition can be cast into the form of an EBK-like rule

$$\tilde{I}_N = (\tilde{n}_N + \tilde{\alpha}_N/4)\hbar \tag{46}$$

by inserting this rule into (40). The quantum number $\tilde{n}_N$ cancels due to the 2π-periodicity of the cosine. Inverting the cosine on the correct branch, which is determined by Π, gives $2q$ "Maslov phase functions"

$$\tilde{\alpha}_N = \frac{2}{\pi}\arg\Big(\cos[2\pi(l-\sigma)/q] + i\Pi\sqrt{\exp(2\Theta/\hbar) + \sin^2[2\pi(l-\sigma)/q]}\Big) + \frac{2}{\pi}\rho, \tag{47}$$

where "arg" extracts the polar angle $\in [0, 2\pi)$ of a complex number. In contrast to the type of classical motion and its characterizing Maslov index α_N, which both change discontinuously at the separatrix, the Maslov phase function varies smoothly across the separatrix. Hence, (33) and (46, 47) do not define a periodic lattice in the entire action space; instead they define a "WKB lattice" in the terminology of [11].

Let us consider first the WKB lattice deep within the resonance zone, $E_N \ll \varepsilon$. From $\Theta \gg \hbar$ and $\rho \approx 0$ follows an EBK rule with constant $\tilde{\alpha}_N = 2 - \Pi$. The l-independence of $\tilde{\alpha}_N$ manifests itself in a q-fold quasi-degeneracy of the eigenvalues $\tilde{I}_N$; $l = 1, \ldots, q$ labels those eigenvalues. Translated into action-space geometry, the EBK rules for $\tilde{I}_1, \ldots, \tilde{I}_N$

give two sets ($\Pi = \pm 1$) of q identical lattices, each set having unique basis and lattice vectors. It is possible to combine both sets to a single lattice with a non-primitive elementary cell, a so-called "quantum cell" invented in [11]. Here, the quantum cell is a N-dimensional cube containing $2q$ quantum states. Going back to the full system, one finds from (19) and (46)

$$I_N = 2\tilde{I}_N = (n_N + 1/2)\hbar \tag{48}$$

with $n_N = 2\tilde{n}_N$ if $\Pi = +1$, and $n_N = 2\tilde{n}_N + 1$ if $\Pi = -1$. We see therefrom that Π is the parity with respect to the potential's symmetry line $\vartheta_N = \pi/q$. The Maslov index 2 in the EBK rule (48) is in agreement with the oscillatory character of the motion of the Nth degree of freedom in this phase space regime.

The other extreme case, $E_N \gg \varepsilon$, well outside the resonance zone, coincides with the unperturbed limit; we have $\Theta \ll -\hbar$ and $\rho \approx 0$ giving

$$\tilde{\alpha}_N = \bar{\Pi}\frac{4}{q}(l - \sigma) \tag{49}$$

$$\text{with } \bar{\Pi} = \frac{\Pi}{\operatorname{sign}\{\sin[2\pi(l-\sigma)/q]\}}.$$

Eigenvalues $\tilde{I}_N$ with different $\bar{\Pi}$ are twofold degenerated in the non-generic situation of 2σ being an integer. The Maslov phase $\tilde{\alpha}_N$ depends on the actions $\tilde{I}_1, \ldots, \tilde{I}_{N-1}$ via $\sigma(A)$ reflecting the non-trivial symmetry reduction. Clearly, the quantization conditions (33) and (46) with (49) give, in general, a non-periodic eigenvalue distribution in the action space of the symmetry reduced system. Nevertheless, we will see in the following that periodic lattices in classically small regions of action space still exist. Each such region, even though classically small, contains many eigenvalues in the semiclassical limit. Here, σ is approximately a linear function of the actions

$$\sigma = b_0 + \sum_{i=1}^{N-1} b_i \tilde{I}_i/\hbar\,. \tag{50}$$

Reformulating the quantization conditions (33) and (46) with the help of (50) gives an equation which compares to (45) (with $\tilde{\boldsymbol{I}}$ and $\tilde{\boldsymbol{n}}$ instead of $\boldsymbol{J}$ and $\boldsymbol{k}$), describing $2q$ lattices with basis vectors $a_{0i} = \tilde{\alpha}_i\hbar/4$ and lattice vectors $a_{ij} = \delta_{ij}\hbar - \delta_{jN}\bar{\Pi}b_i\hbar/q$ if $i < N$, else $a_{0N} = \bar{\Pi}(l - b_0)\hbar/q$ and $a_{Nj} = \delta_{Nj}\hbar$. For fixed $\bar{\Pi}$ and l, the lattice vectors have, in general, different lengths and are not orthogonal; the lattice is N-dimensional triclinic. Note that, in general, a single quantum cell cannot be defined due to non-matching lattice vectors. The reader should realize that the unperturbed eigenvalues of both the full and the symmetry reduced system lie on a simple N-dimensional cubic lattice in the respective "correct" action space: for the symmetry reduced system, the quantum analog of the classical elastic reflections are Dirichlet boundary conditions, i. e. vanishing wave function, on the lines $\vartheta_N = 0$ and $\vartheta_N = \pi/q$ leading to an EBK rule with Maslov index 4 (a hard wall instead of a smooth turning point increases the Maslov index by 1). For the full system, we get an EBK rule from (46) and (49) using (38)

$$I_N = \Lambda q\tilde{I}_N + A = (n_N + \alpha_N/4)\hbar \tag{51}$$

with the identifications $\bar{\Pi} = -\Lambda$ and $n_N = -\Lambda q\tilde{n}_N - l$. In the unperturbed case, the quantum index $\bar{\Pi}$ therefore equals the classical index $-\Lambda$ which characterizes the parts outside the resonance zone. It is thus possible to relate each quantum wave function Ψ uniquely to the classical $\Lambda = +1$-region or the $\Lambda = -1$-region. At finite $E_N > \varepsilon$, there is no unique relation between quantum states and these classical regions as already discussed. When representing the eigenvalues of the exterior of the resonance zone in the action space of the full system ($\boldsymbol{I}$- or $\boldsymbol{L}$-space), we project into the $\Lambda = +1$-region (we could also choose the $\Lambda = -1$-region). In this "reduced action space" the eigenvalues lie on N-dimensional cubic lattices; see (33) and (51).

3.3. Example: Coupled Rotors

We return to the example of two coupled rotors (25) with $\boldsymbol{m} = (-1, 1)$. The Maslov indices of free rotors, β_j, vanish, such as the transformed ones, α_j, do. Combining with $A = P_1/2$ we get $\sigma = -I_1/(2\hbar) = -n_1/2$. This linear dependence makes for globally periodic lattices outside the resonance zone in $\tilde{\boldsymbol{I}}$-space. These lattices with basis vectors $\boldsymbol{a}_0 = (0, \bar{\Pi}l\hbar/q)$ and lattice vectors $\boldsymbol{a}_1 = (\hbar, \bar{\Pi}\hbar/(2q))$, $\boldsymbol{a}_2 = (0, \hbar)$ are skewed. Because of the integer-valuedness of 2σ, the lattices with $\bar{\Pi} = +1$ and the ones with $\bar{\Pi} = -1$ are congruent, or in other words, the eigenvalues are twofold degenerated.

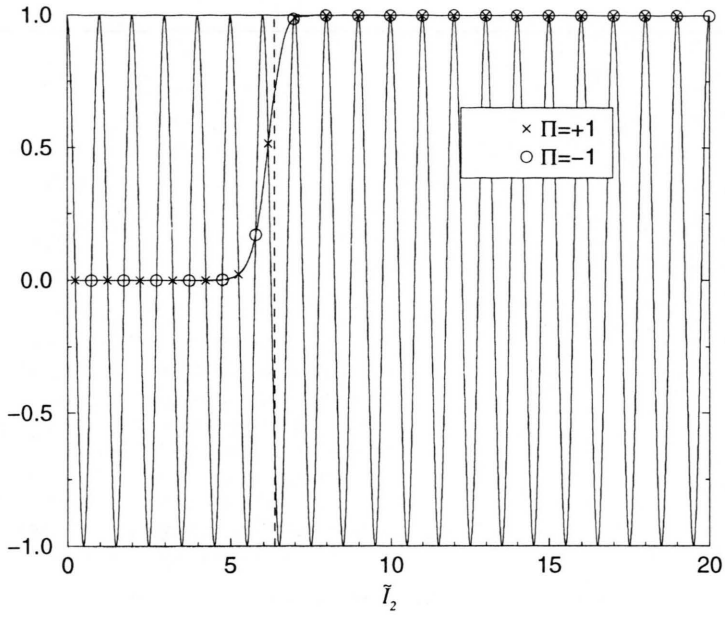

Fig. 13. Graphical solution of the quantization condition (40) for two coupled rotors with $\boldsymbol{m} = (-1, 1)$, $q = 1$, $\varepsilon = 0.02$, and n_1 even. Each side of (40) is drawn as a function of $\tilde{I}_2 = \phi\hbar/(2\pi)$ in units of $\hbar = 0.02$; intersection points indicate quantized values of $\tilde{I}_2$. The dashed line marks the separatrix $\tilde{I}_2 = \Delta I/2$.

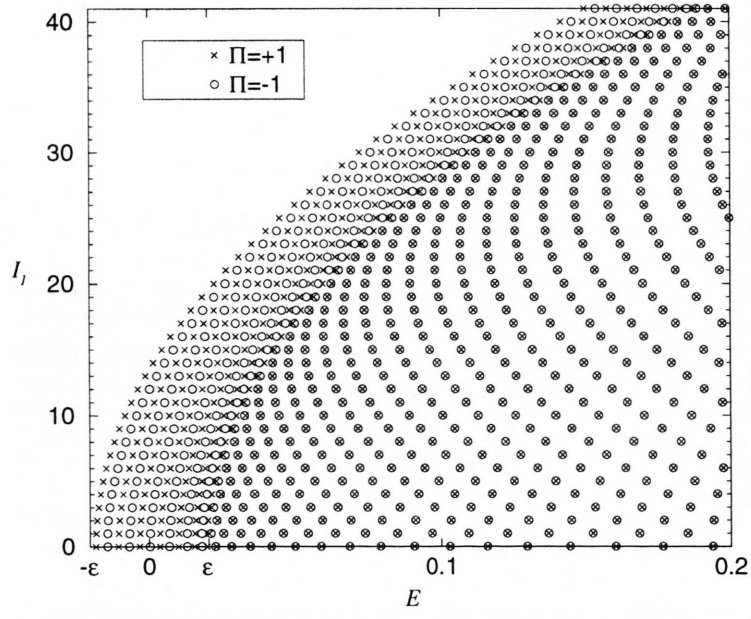

Fig. 14. Semiclassical eigenvalues of two coupled rotors with $\boldsymbol{m} = (-1, 1)$, $q = 1$ and $\varepsilon = 0.02$ in the space of the energy E and action $I_1 = J_1 + J_2$ (in units of $\hbar = 0.02$). The symmetric region of negative I_1 is omitted.

Before studying the model with $q = 1$ in detail, it is interesting to mention that this model has already been treated in Born's 1925 book *Vorlesungen über Atommechanik* [34] with the old Bohr-Sommerfeld quantization rules (EBK without Maslov indices). This is a too crude approximation as it will become apparent in the following. Consider the right hand side of the quantization condition (40). It is positive or negative, depending on whether n_1 is even or odd. Figure 13 illustrates the former situation (for odd n_1 the non-periodic curve is reflected at the zero line). The action $\tilde{I}_2$ is discretized according to (48) in the small-$\tilde{I}_2$ domain (deep within the resonance zone) and according to (46) and (49) with twofold degeneracy

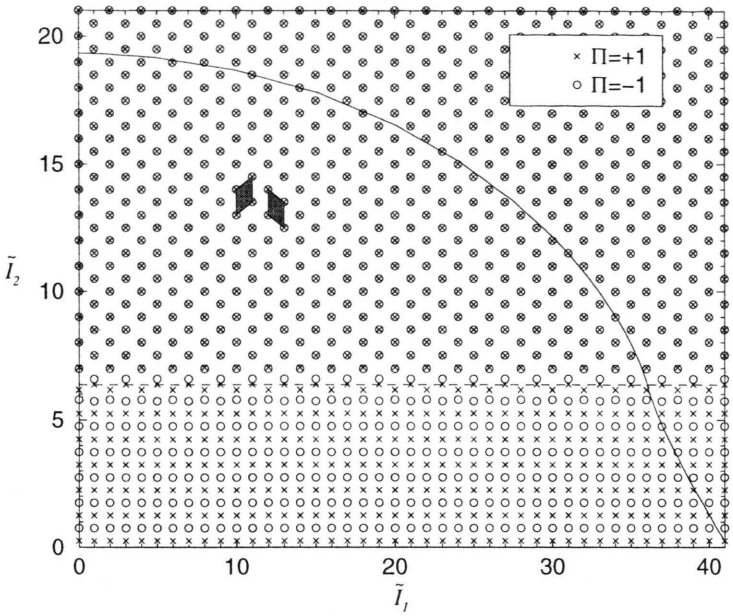

Fig. 15. Semiclassical eigenvalues of two coupled rotors with $\boldsymbol{m}\,(-1,1)$, $q=1$ and $\varepsilon = 0.02$ in $\tilde{\boldsymbol{I}}$-space in units of $\hbar = 0.02$. The symmetric region of negative action $\tilde{I}_1$ is omitted. The solid line is the energy surface $E = 0.15$, and the dashed line is the separatrix surface. Filled regions represent elementary cells belonging to $\bar{\Pi} = +1$ (left) and $\bar{\Pi} = -1$ (right).

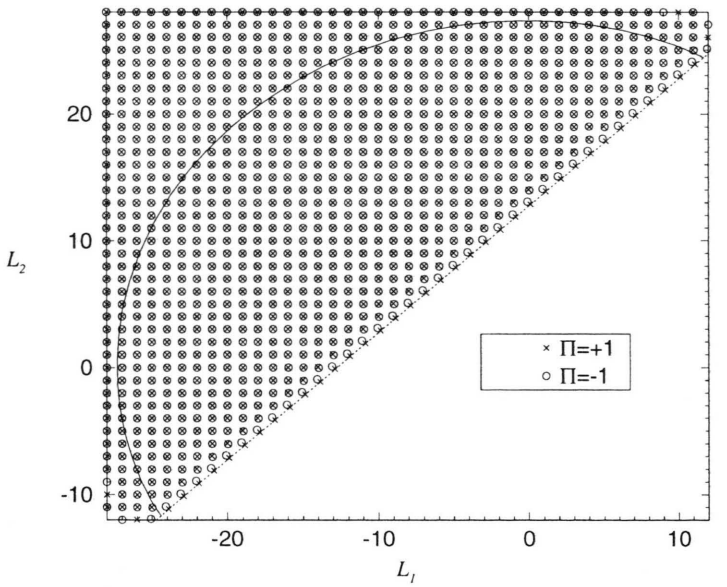

Fig. 16. Semiclassical eigenvalues of two coupled rotors with $\boldsymbol{m}\,(-1,1)$, $q=1$ and $\varepsilon = 0.02$ in reduced $\boldsymbol{L}$-space in units of $\hbar = 0.02$. Eigenvalues belonging to the resonance zone are not shown. The solid line is the energy surface $E = 0.15$ and the dashed line is the separatrix surface.

in the large-$\tilde{I}_2$ domain (well outside the resonance zone). The transition between these different kinds of discretization happens in a narrow region around the separatrix with width of order $\hbar$.

Solving quantization condition (40) for all values of n_1 gives the complete set of eigenvalues. Figure 14 shows their arrangement in the space of the constants of motion E and $I_1 = J_1 + J_2$. The twofold quasi-degeneracy at large energies is related to the exact degeneracy of the unperturbed eigenvalues $E = (k_1^2 + k_2^2)\hbar^2/2$ and $I_1 = (k_1 + k_2)\hbar$. The eigenvalue pattern looks rather regular due to the fact that one constant of motion is an action variable. However, the underlying regular structures are more transparent in the $\tilde{\boldsymbol{I}}$-representation in Figure 15. The eigenvalues are located on the WKB lattice, which reduces to periodic lattices far away from the separatrix surface. Below the separatrix, i. e. inside the resonance zone, the eigen-

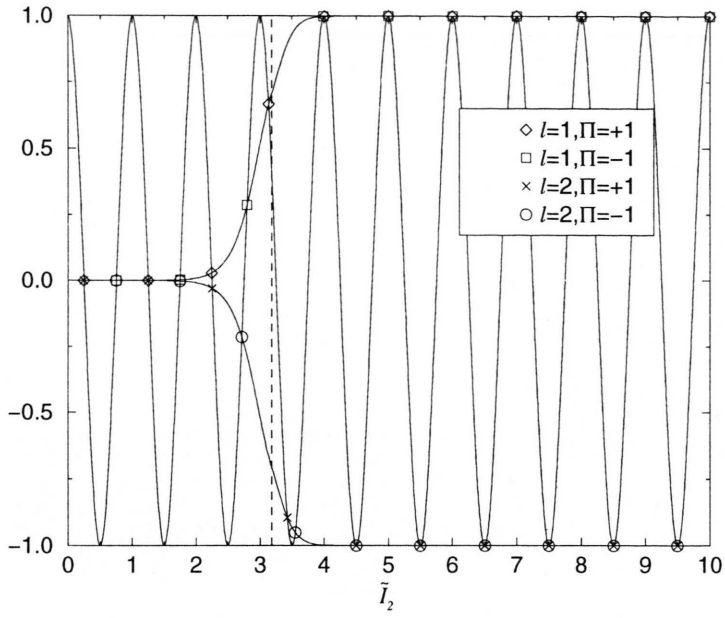

Fig. 17. Graphical evaluation of (40) for two coupled rotors with $\boldsymbol{m}$ $(-1, 1)$, $q = 2$, $\varepsilon = 0.02$, $\hbar = 0.02$, and $n_1/2$ even. The dashed line marks the separatrix.

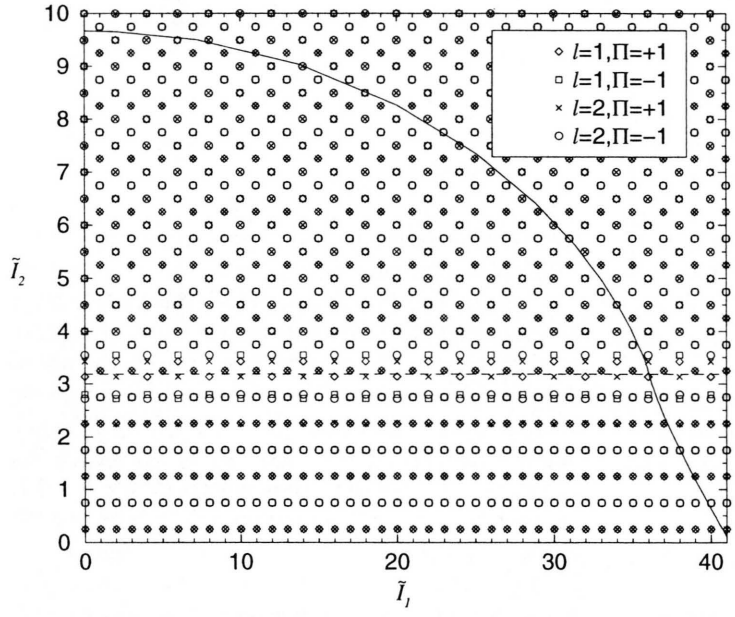

Fig. 18. Semiclassical eigenvalues of two coupled rotors with $\boldsymbol{m}$ $(-1, 1)$, $q = 2$, $\varepsilon = 0.02$, and $\hbar = 0.02$ in $\tilde{\boldsymbol{I}}$-space. The solid line is the energy surface $E = 0.15$, and the dashed line is the separatrix surface.

values lie on two quadratic lattices. It is here trivial to see how a larger square elementary cell (the quantum cell) could combine both lattices to a single one. Above the separatrix, i. e. outside the resonance zone, twofold degenerated eigenvalues lie on two different but congruent skewed lattices, the elementary cells of which are illustrated in Figure 15. The integer-valuedness of 2σ ensures here the existence of a quantum cell, a body-centred square in the terminology of crystallography. As the separatrix surface is crossed from above, a smooth, degeneracy-lifting transition to the quadratic lattices takes place. The lattice outside the resonance zone is even simpler when projected into the $\Lambda = +1$-region of $\boldsymbol{L}$-space

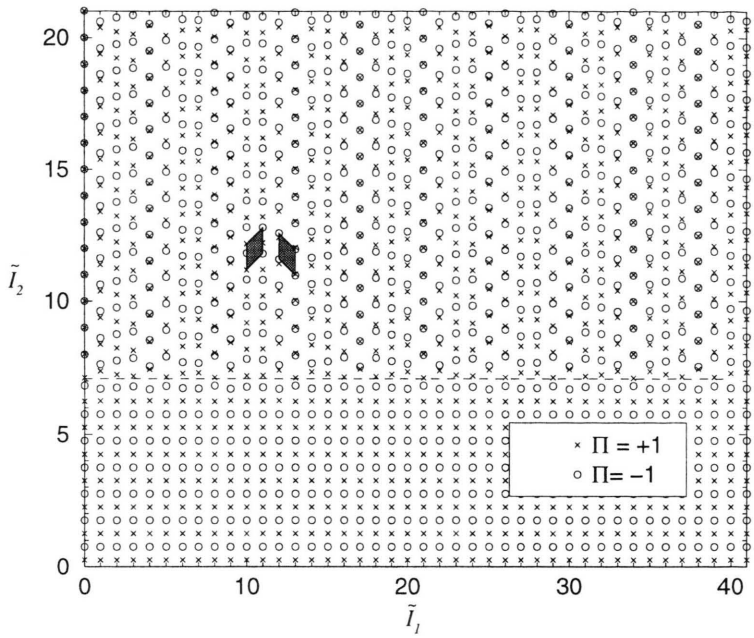

Fig. 19. Semiclassical eigenvalues of two coupled non-identical rotors with irrational $\sigma, \boldsymbol{m}\,(-1,1), q = 1, \varepsilon = 0.02$, and $\hbar = 0.02$ in $\tilde{\boldsymbol{I}}$-space. The dashed line marks the separatrix surface. Filled regions represent elementary cells belonging to $\bar{\Pi} = +1$ (left) and $\bar{\Pi} = -1$ (right).

as displayed in Figure 16. Away from the separatrix surface, twofold-degenerate eigenvalues are arranged on quadratic lattices according to the EBK rule of the unperturbed system (33) and (51). The price to pay for recovering a simple lattice for a subset of eigenvalues is the loss of the coherent picture of the action-space discretization as shown in Figure 15.

Let us now discuss the case $q = 2$. The quantization condition (40) simplifies to an EBK rule if its right hand side vanishes. This is the case if n_1 is odd since $\sigma = -n_1/2$. In the more complicated case of n_1 even, we have to distinguish between $n_1/2$ even and $n_1/2$ odd. Figure 17 illustrates the former situation. Note that the sign of the right hand side of the quantization condition is determined by l. (For odd $n_1/2$ the solutions to $l = 1$ and $l = 2$ are interchanged.) We see here in addition to the twofold degeneracy for large $\tilde{I}_2$ also a twofold degeneracy for small $\tilde{I}_2$. Figure 18 shows that above the separatrix surface the lattice in action space looks similar to $q = 1$ in Figure 15. However, the situation now is actually a bit more involved: two kinds of elementary cells labelled by $\bar{\Pi} = \pm 1$ are shifted by $\hbar/2$ in $\tilde{I}_2$-direction ($l = 1, 2$); we have four lattices instead of two. Again, a quantum cell could be defined. A more striking difference between the case $q = 1$ in Fig. 15 and $q = 2$ in Fig. 18 is that in the latter case there is a twofold degeneracy below the separatrix surface.

Finally, we illustrate a more generic case with irrational σ using two coupled non-identical rotors as example

$$H_0 = \frac{1}{2}J_1^2 + \frac{\gamma}{2}J_2^2\,, \tag{52}$$

with γ being the reciprocal of the golden mean, $(\sqrt{5}-1)/2$. We again take $\boldsymbol{m} = (-1, 1)$ and $q = 1$ giving $\sigma = -n_1/(1+\gamma)$. Figure 19 confirms that the quadratic lattices below the separatrix surface are as in the case of integer-valued 2σ pictured in Figure 15. But above the separatrix surface, there are two non-congruent skewed lattices with basis vectors $\boldsymbol{a}_0 = (0, \bar{\Pi}\hbar)$ and lattice vectors $\boldsymbol{a}_1 = (\hbar, \bar{\Pi}\hbar/(1+\gamma))$, $\boldsymbol{a}_2 = (0, \hbar)$. A quantum cell does not exist in this case, which is expressed by the seeming irregularity of the overlap of the lattices in Figure 19. Note that the eigenvalues in Fig. 19 are distinguished by their quantum number Π and not by the lattice index $\bar{\Pi}$.

3.4. Energy-level Statistics

Let us discuss the implications of the observed lattice structures on the statistical properties of the energy levels in the semiclassical limit $\hbar \to 0$. For generic simple systems with two and more degrees of freedom it has been proven by Berry and

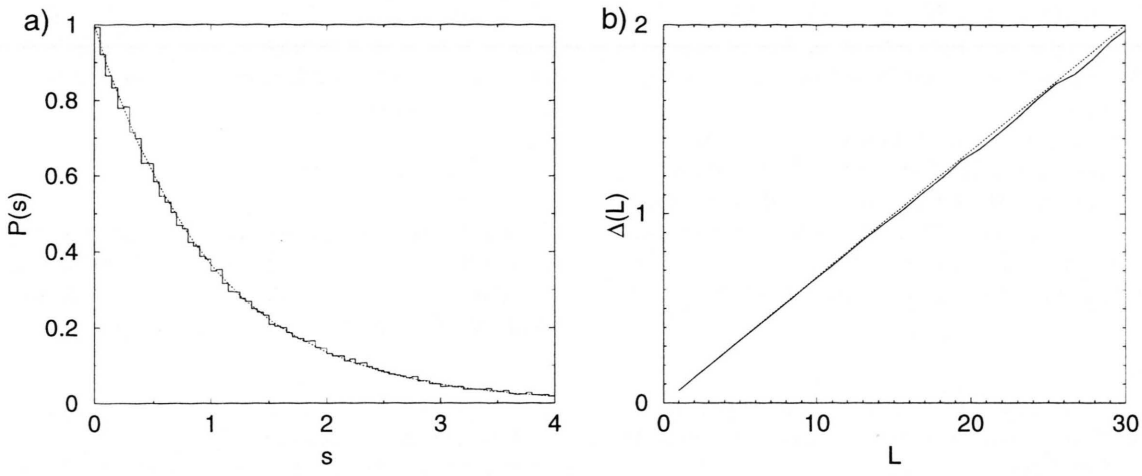

Fig. 20. Energy-level statistics of the first 98192 levels with $\Pi = -1, \hbar = 0.004$ and the other parameters as in Figure 19. The data are well fitted by the Poisson distribution (dotted lines). a) Nearest-neighbor distribution $P(s)$. b) Spectral rigidity $\Delta(L)$.

Tabor [35] that the distribution of spacings between adjacent levels (after unfolding the spectrum such that the mean level spacing is unity) is given by $P(s) = \exp(-s)$, indicating Poisson-distributed, i. e. randomly distributed, levels. This has been confirmed numerically for a variety of simple systems and also for higher-order correlations; see [36] for a review.

The starting point in the proof [35] is the EBK rule which is not valid for nonsimple systems. However, the following heuristic argument shows that generic classically integrable systems should also have Poisson-distributed energy levels. Apart from small regions close to separatrices, the local lattice structure of the eigenvalues in the action space of the full system is approximately EBK-like; see e. g. Figure 16. So, essentially, we have a superposition of a finite number of uncorrelated sets of randomly distributed levels. This results in a Poisson distribution. Surprisingly, this has only been checked so far for the elliptic billiard [37]. After separating the spectrum according to parities, the nearest-neighbor statistics $P(s)$ and the spectral rigidity $\Delta(L)$ has been found to be consistent with the Poisson distribution. The spectral rigidity is the mean square deviation of the spectral staircase from the straight line that best fits over a range of L mean level spacings [38, 39]; $\Delta(L) = L/15$ for Poisson-distributed levels. An example of our numerical results is shown in Figure 20. It confirms quite convincingly that energy levels of nonsimple integrable systems are Poisson-distributed.

4. Conclusions

The classical and quantum mechanics of isolated, nonlinear resonances has been presented in action space. The energy surfaces were found to be typically composed of two different kinds of patches corresponding to the inner and the outer part of the resonance zone. The graphical representation of these surfaces for a model of coupled rotors proved to be a very concise description of the integrable dynamics. Moreover, it was demonstrated that energy surfaces outside the resonance zone can be approximated by canonical perturbation theory, but have to be handled with care, since non-physical segments are produced close to the resonance zone.

Exploiting the one-component property of the system, we have investigated the distribution of the quantum mechanical eigenvalues in the action space of the symmetry reduced system: the eigenvalues within the resonance zone are located on N-dimensional cubic lattices, whereas the other eigenvalues are located on locally N-dimensional triclinic lattices. The skewness of the latter lattices was traced back to a nontrivial symmetry reduction. This more general kind of symmetry reduction does not only reduce phase space area by a factor, it also shifts its value by a constant. Both kinds of lattices and the smooth transition between them were described by a uniform semiclassical quantization procedure and graphically illustrated with the help of the coupled-rotor model.

It was found that simple cubic lattices can be recovered only separately for each of the different types of classical motion in a properly reduced action space of the full system.

We have presented an heuristic argument showing that the energy-level statistics of the systems discussed here should be Poisson distributed, despite of the complex lattice structure of their eigenvalues. We confirmed this with our numerical data by computing the nearest-neighbor statistics and the spectral rigidity.

The presented discussion deals with nonlinear resonances. The important linear case of coupled harmonic oscillators demands special considerations in a future publication.

Acknowledgement

I wish to thank P. H. Richter for attracting my attention to this subject and his support during my PhD studies. H. Waalkens and O. Zaitsev are acknowledged for critically reading the manuscript.

[1] P. H. Richter, Die Theorie des Kreisels in Bildern, Report 226, Institut für Dynamische Systeme, Universität Bremen 1990.
[2] H. R. Dullin, M. Juhnke, and P. H. Richter, Int. J. Bifurcation and Chaos **4**, 1535 (1994).
[3] H. R. Dullin and A. Wittek, J. Phys. A **27**, 7461 (1994).
[4] P. H. Richter, A. Wittek, M. P. Kharlamov, and A. P. Kharlamov, Z. Naturforsch. **50a**, 693 (1995).
[5] O. Heudecker, Teilchenbewegung in der Kerr-Raumzeit, Dissertation, Universität Bremen 1995.
[6] J. Wiersig and P. H. Richter, Z. Naturforsch. **51a**, 219 (1996).
[7] P. H. Richter, H. R. Dullin, H. Waalkens, and J. Wiersig, J. Phys. Chem. **100**, 19124 (1996).
[8] H. R. Dullin, O. Heudecker, M. Juhnke, H. Pleteit, H.-P. Schwebler, H. Waalkens, J. Wiersig, and A. Wittek, Energy Surfaces in Action Space, Report 406, Institut für Dynamische Systeme, Universität Bremen 1997.
[9] J. Wiersig, Int. J. Bifurcation and Chaos **10**, 2075 (2000).
[10] J. Wiersig, Die klassische und quantenmechanische Beschreibung integrabler Hamiltonscher Systeme im Wirkungsraum, Shaker Verlag, Aachen 1998; Dissertation.
[11] H. Waalkens, J. Wiersig, and H. R. Dullin, Ann. Phys. New York **276**, 64 (1999).
[12] A. N. Kolmogorov, General Theory of Dynamical Systems and Classical Mechanics, Proc. of the 1954 Intern. Congress Math., Amsterdam 1957, p. 315-333.
[13] V. I. Arnol'd, Russ. Math. Surveys **18**, 85 (1963).
[14] J. Moser, Nachr. Akad. Wiss. Göttingen, Math. Phys. Kl., 1962, p. 1-20.
[15] B. V. Chirikov, Phys. Rep. **52**, 263 (1979).
[16] A. J. Lichtenberg and M. A. Lieberman, Regular and Chaotic Dynamics, Springer-Verlag, Berlin 1992.
[17] E. L. Sibert, J. T. Hynes, and W. P. Reinhardt, J. Chem. Phys. **77**, 3595 (1982).
[18] A. Einstein, Verh. DPG *19*, 82 (1917).
[19] J. B. Keller, Ann. Phys. **4**, 180 (1958).
[20] H. Waalkens, J. Wiersig, and H. R. Dullin, Ann. Phys. New York **260**, 50 (1997).
[21] Herbert Goldstein, Classical Mechanics, 2. ed., Addison-Wesley, Reading, MA 1980.
[22] V. I. Arnol'd. Mathematical Methods of Classical Mechanics, Graduate Texts in Mathematics Vol. 60, Springer-Verlag, Berlin 1978.
[23] J. M. Robbins and R. G. Littlejohn, Phys. Rev. Lett. **58**, 1388 (1987).
[24] G. J. Rieger, Zahlentheorie, Vandenhoeck & Ruprecht, Göttingen 1976.
[25] R. Aldrovandi and P. Leal Ferreira, Amer. J. Phys. **48**, 660 (1980).
[26] I. S. Gradshteyn and I. M. Ryzhik, Tables of Integrals, Series, and Products, Academic Press, New York 1965.
[27] Paul F. Byrd and Morris D. Friedman, Handbook of Elliptic Integrals for Engineers and Physicists, Springer-Verlag, Berlin 1971.
[28] V. P. Maslov, Théorie des Perturbations et Méthodes Asymptotiques, Dunod, Paris 1972.
[29] A. M. Ozorio de Almeida, J. Phys. Chem. **88**, 6139 (1984).
[30] W. H. Miller, J. Chem. Phys. **48**, 1651 (1968).
[31] J. N. L Connor, T. Uzer, and R.+A. Marcus, J. Chem. Phys. **80**, 5095 (1984).
[32] Y. Ayant and R. Arvieu, J. Phys. A **20**, 397 (1987).
[33] M. Sieber, J. Phys. A, **30**, 4563 (1997).
[34] M. Born, Vorlesungen über Atommechanik, Springer-Verlag, Berlin 1925.
[35] M. V. Berry and M. Tabor, Proc. Roy. Soc. London A **356**, 375 (1977).
[36] M. Robnik and G. Veble, J. Phys. A **31**, 4669 (1998).
[37] R. van Zon and T. W. Ruijgrok. Eur. J. Phys. **19**, 77 (1998).
[38] M. L. Mehta, Random Matrices and the Statistical Theory of Energy Levels, Academic Press, New York 1967.
[39] M. V. Berry, Proc. Roy. Soc. Lond. A, **400**, 229 (1985).